JGR Solid Earth

RESEARCH ARTICLE
10.1029/2021JB021743

A New Tectonic Model Between the Madagascar Ridge and Del Cano Rise in the Indian Ocean

Taichi Sato[1], Yoshifumi Nogi[2,3], Hiroshi Sato[4], and Masakazu Fujii[2,3]

[1]Geological Survey of Japan, AIST, Tsukuba, Ibaraki, Japan, [2]Geoscience Group, National Institute of Polar Research, Tachikawa, Tokyo, Japan, [3]Department of Polar Science, School of Multidisciplinary Sciences, The Graduate University for Advanced Studies, SOKENDAI, Tachikawa, Tokyo, Japan, [4]Department of Business Administration, Senshu University, Kawasaki, Kanagawa, Japan

Abstract The southern Indian Ocean has several prominent aseismic ridges recognized as oceanic large igneous provinces (i.e., the Madagascar Ridge, Del Cano Rise, Crozet Plateau, and Conrad Rise) in the off-axis areas of the Southwest Indian Ridge (SWIR). However, previously obtained magnetic survey lines are sparse and not correctly aligned with the seafloor spreading direction; thus, the detailed spreading history, including the formation of these aseismic ridges, remains an open question. We reconstructed the tectonic history of two segments between the Discovery II and Gallieni fracture zones in the SWIR using newly obtained magnetic data (total and vector magnetic field) and an open-source magnetic data set. We revealed that the southern Madagascar Ridge and the Del Cano Rise once formed a single bathymetric high and separated by at least Chron 30y, which is quite different from the global age model. In addition, the rises may have formed before Chron 34y, assuming an extinct ridge south of the Del Cano Rise. The two rises have been recognized as having formed by Marion hotspot plume-induced excess volcanism around the active spreading ridge of the SWIR, which can explain locally isostatically compensated thicker-than-normal crust. However, linear magnetic anomalies have not been observed across the main part of these rises, suggesting that magmatic activity controlled by seafloor spreading is unlikely. Like other aseismic ridges in the southern Indian Ocean, these two rises may possibly have been formed partly by continental fragments rather than plume-induced excess volcanism.

Plain Language Summary The southern Indian Ocean contains several bathymetric high regions previously interpreted as oceanic large igneous provinces. Hotspot-ridge interaction is considered as the key factor in the formation of such large volcanic structures. However, the detailed seafloor spreading history and origin of these large volcanic structures are not understood as well as those in other oceans because of the vast and remote Indian Ocean. We conducted magnetic surveys and reconstructed a new tectonic history of two segments along the Southwest Indian Ridge (SWIR). We found that the southern Madagascar Ridge and the Del Cano Rise once formed a single bathymetric high and that they separated by at least 66 million years ago. Moreover, the rises may have formed before 84 million years ago, assuming an extinct ridge south of the Del Cano Rise. The two rises might have formed by interaction between the Marion hotspot and SWIR; however, linear magnetic anomalies implying seafloor spreading are not observed in the main parts of these rises. This absence suggests that hotspot-ridge interaction cannot fully explain the origin of these rises. We cannot exclude the possibility that the two rises are partly continental fragments rather than products of hotspot-induced excess volcanism.

Key Points:

- Revised seafloor ages up to Chron 31 in the Indian Ocean are obtained by new total and vector magnetic data
- Our new tectonic scenario indicates that the Madagascar Plateau and Del Cano Rise once formed a single bathymetric high
- The tectonics of oceanic plateaus in the Indian Ocean need to be reexamined, including continental fragment origin

Supporting Information:

Supporting Information may be found in the online version of this article.

Correspondence to:

T. Sato,
taichi-sato@aist.go.jp

Citation:

Sato, T., Nogi, Y., Sato, H., & Fujii, M. (2022). A new tectonic model between the Madagascar Ridge and Del Cano Rise in the Indian Ocean. *Journal of Geophysical Research: Solid Earth*, *127*, e2021JB021743. https://doi.org/10.1029/2021JB021743

Received 23 JAN 2021
Accepted 18 DEC 2021

Author Contributions:

Conceptualization: Taichi Sato, Yoshifumi Nogi, Hiroshi Sato, Masakazu Fujii
Data curation: Taichi Sato
Formal analysis: Taichi Sato
Funding acquisition: Yoshifumi Nogi
Investigation: Taichi Sato, Yoshifumi Nogi, Hiroshi Sato, Masakazu Fujii
Project Administration: Yoshifumi Nogi
Resources: Yoshifumi Nogi
Supervision: Yoshifumi Nogi
Visualization: Taichi Sato
Writing – original draft: Taichi Sato
Writing – review & editing: Yoshifumi Nogi, Hiroshi Sato, Masakazu Fujii

1. Introduction

The Indian Ocean is among the best locations worldwide for understanding the supercontinent fragmentation process because the seafloor spreading history following the breakup of Gondwana is still observable (Figure 1). Many seafloor spreading models of the Indian Ocean have already been presented (e.g., Norton & Sclater, 1979; Royer & Sandwell, 1989; Zahirovic et al., 2012). In the southwestern Indian Ocean, the seafloor is dominated by the Southwest Indian Ridge (SWIR) and several aseismic ridges (e.g., the Madagascar Ridge, Del Cano Rise, and Conrad Rise) and hotspots (e.g., Marion and Crozet). These aseismic ridges have been listed as oceanic large igneous provinces (LIPs; e.g., Bryan & Ernst, 2008; Coffin & Eldholm, 1994). Many magnetic surveys have been conducted; however, previously obtained magnetic survey lines are sparse and not properly aligned for detecting

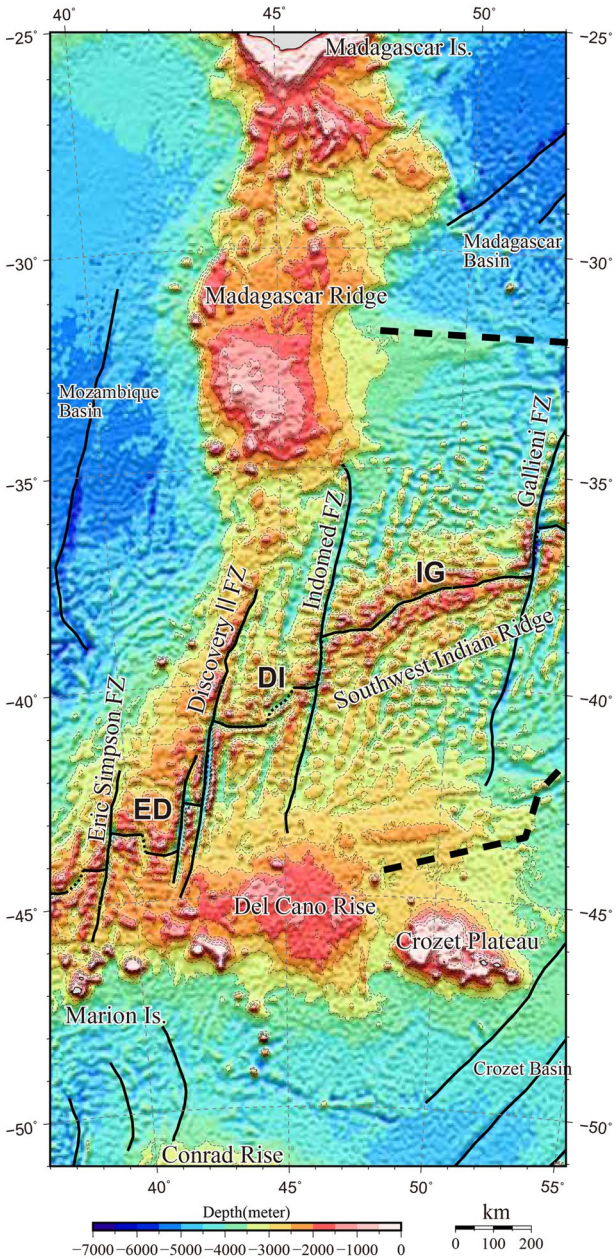

Figure 1. Regional map of the survey area. The background image uses ETOPO-1 global topography (Amante & Eakins, 2009). The solid black lines indicate the Southwest Indian Ridge (SWIR), transform faults, and primary fracture zone traces extracted from the satellite-based free-air gravity anomaly and vertical gravity gradient (Sandwell et al., 2014; Figure S1). The dashed black lines show triple junction traces on the African and Antarctic Plates (Patriat & Ségoufin, 1988; ED: Eric Simpson-Discovery II segment; DI: Discovery II-Indomed segment; IG: Indomed-Gallieni segment). The thin dashed lines are bathymetric contours at 500-m intervals.

the seafloor spreading direction (Figure 2). Therefore, the detailed seafloor spreading history of this area, including the formation of these aseismic ridges, is still an open question.

Satellite-based free-air gravity anomalies (Sandwell et al., 2014) are a powerful tool for understanding the tectonic settings of aseismic ridges. For example, volcanic islands such as the Hawaiian Islands generally have positive anomalies surrounded by negative anomalies, which can be explained by the simple flexure of the oceanic plate due to crustal loading of excess material. In contrast, the Tamu Massif, which is the main edifice of the Shatsky Rise (another oceanic LIP), does not show a gravity signature with a large mass concentration at the center but has small gravity anomalies of <30 mGal. The massif is almost completely isostatically compensated, and Sager et al. (2019) identified linear magnetic anomalies on the massif. They proposed that the massif was formed by voluminous and focused ridge volcanism rather than a shield volcano emplaced on preexisting oceanic crust.

In the southern Indian Ocean, islands south of the SWIR such as the Prince Edward Islands and the Crozet Islands have positive anomalies surrounded by negative anomalies. This gravity signature implies excess volcanism on preexisting oceanic crust similar to that of the Hawaiian shield volcanoes. In contrast, the southern Madagascar Ridge and Del Cano Rise, which are located the off-axis of the SWIR to the north and south, respectively, are characterized by only positive gravity anomalies between 30 and 90 mGal (Figure 2a). This implies that a large central mass concentration on the preexisting oceanic crust as for shield volcanoes is an unlikely explanation of their origin. Both rises have been estimated to have a crustal thickness of over 10 km (Goslin & Diament, 1987; Schlich, 1982), and they have been classified as oceanic LIPs. They have been proposed to have originated from anomalous volcanism caused by the reorganization of plate kinematics near the active SWIR because their gravity anomalies are partly isostatically compensated (Goslin & Diament, 1987). Global gravity and seafloor spreading models have also led to the proposal of Marion hotspot-SWIR interaction as a formation mechanism for the Del Cano Rise (e.g., Georgen et al., 2001; Zhang et al., 2011). Previous studies have suggested that the tectonic settings of the southern Madagascar Ridge and Del Cano Rise differ from that of the Crozet Plateau, but the origins of the two rises are still under debate. Goslin et al. (1981) proposed that the southern Madagascar Ridge and the Crozet Plateau (in their paper, the Crozet Plateau was defined as a larger bathymetric high including the Del Cano Rise) probably have a common origin based on their magnetic anomalies, although this idea was based on sparse seafloor age identifications which were the only ones available at that time. Therefore, a more detailed seafloor spreading history around these rises is essential for reconstructing the separation history between the two rises and for improving the Late Cretaceous seafloor spreading history, including the nature of aseismic ridges and hotspots in the central Indian Ocean.

We recently conducted several geomagnetic surveys at the SWIR between the Discovery II and Gallieni fracture zones (FZs). The survey lines were planned to align with the spreading direction of the SWIR. We combined our data with previous magnetic data to reestimate the seafloor age and reconstruct a seafloor spreading model. We evaluated the gravity and magnetic signatures to clarify the origins of the southern Madagascar Ridge and Del Cano Rise.

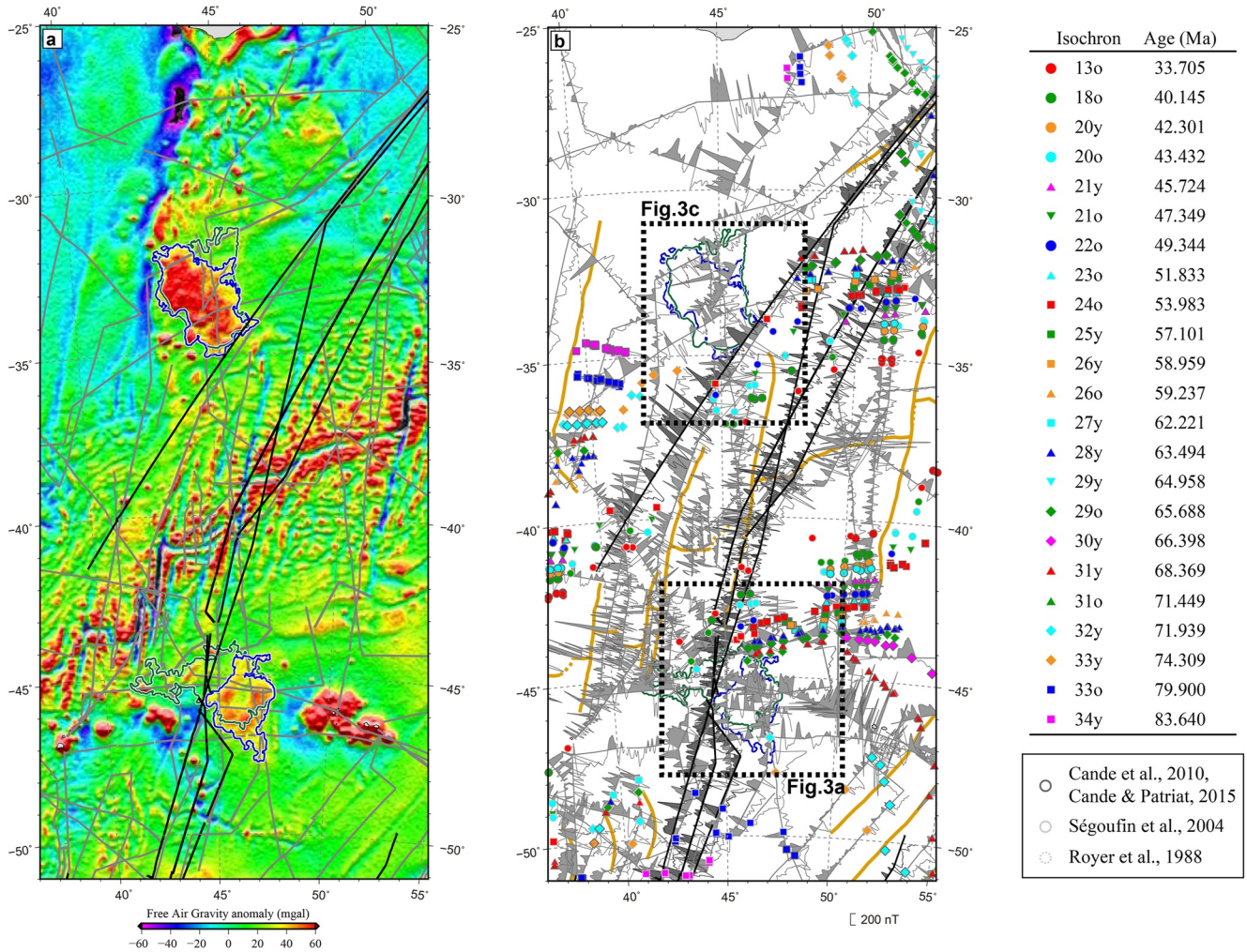

Figure 2. (a) Regional free-air gravity map of the survey area extracted from the satellite-based free-air gravity anomaly (Sandwell et al., 2014). The thick black and gray lines are from our magnetic survey and other magnetic surveys, respectively. The thick green lines around the southern part of the Madagascar Ridge and Del Cano Rise indicate seafloor depth of <2,000 m. The thick blue lines around the southern part of the Madagascar Ridge and Del Cano Rise indicate free-air gravity anomalies greater than 30 mGal. (b) Magnetic anomaly map of the survey area. Previously identified isochrons are overlain on the profiles. The geomagnetic polarity reversal time scale of Ogg (2012) was used. The solid orange lines indicate the Southwest Indian Ridge (SWIR), transform faults, and primary fracture zone traces. Dashed black rectangular areas encompass the areas shown in Figure 3.

2. Geological Setting

The SWIR is an ultraslow-spreading ridge (spreading rate of 15–17 km/Ma from west to east (e.g., MORVEL; DeMets et al., 2010)) that extends from the Bouvet triple junction to the Rodrigues triple junction. It has a length of ~7,700 km and accounts for 11–12% of the total length of the world's mid-ocean ridges. The survey area was the central SWIR between 35°E and 55°E and included a vast off-axis area ~1,000 km from the spreading axis (Figure 1) containing several remarkable seafloor structures, such as the Madagascar Ridge, Del Cano Rise, Crozet Plateau, Conrad Rise, Prince Edward Islands, and Marion Island. On the basis of vertical gravity gradient (VGG) data (Sandwell et al., 2014; Figure S1), MacLeod et al. (2017) proposed that there may be an extinct ridge trending in an WNW-ESE direction between the Del Cano and Conrad Rises. The survey area contained four major FZs: Eric Simpson, Discovery II, Indomed, and Gallieni, from west to east. Applying the segmentation naming rule of Hosford et al. (2003), we can refer to the first-order segments of the SWIR by using the initials of the two nearest transform faults: ED, DI, and IG. The DI segment comprises two second-order segments with lengths of 135 and 90 km. These are bounded by a nontransform discontinuity with a left-lateral offset that is ~85-km long. The IG segment is ~560-km long, and it has been extensively surveyed (e.g., Mendel et al., 2003; Niu et al., 2015; Sauter et al., 2001, 2009; Zhang et al., 2013; Zhao et al., 2013). The IG segment has been inferred

to have both a thicker crust and hotter mantle than adjacent ridge sections based on the regional axial depth, mantle Bouguer anomalies, geochemical proxies for the degree of mantle melting, and seismic tomographic imagery along the SWIR (Sauter et al., 2009). Thus, locally anomalous melting of the SWIR may be attributed to a regionally higher mantle temperature provided by the Crozet hotspot (Sauter et al., 2009; Zhang et al., 2013). In this study, we defined the southern Madagascar Ridge and Del Cano Rise as bathymetric highs covering areas with free-air gravity anomalies greater than 30 mGal (Figure 2a), which mostly correspond to seafloor depths of <2,000 m (Figure 1). Although an area is better defined by its seafloor depth or morphological characteristics, we chose to use the gravity signature because of our focus on gravity signatures and the ambiguity of the boundaries between these features and their surroundings.

The Madagascar Ridge is an elongated ridge trending in the north-south direction that extends south of Madagascar Island between 26°S and 36°S with a maximum width of ~600 km (Figure 1). The Madagascar Ridge continues south to the northern flanks of the oceanic crust created at the SWIR. The Madagascar Ridge is bounded to the west by the Mozambique Basin and to the east by the Madagascar Basin. The western flank facing the Mozambique Basin is steep and nearly rectilinear. In contrast, the eastern slope facing the Madagascar Basin is gentler with an average distance of 160 km between the 2,000-m and 4,000-m isobaths (Schlich, 1982). According to the global seafloor age model, this ridge was emplaced before ~70 Ma (Müller et al., 2016), but no previous studies have identified any isochrons (Cande & Patriat, 2015; Cande et al., 2010; Royer et al., 1988; Ségoufin et al., 2004; Figure 2b). The Madagascar Ridge is divided into two different domains with the transition along 31°S (Goslin et al., 1981). The northern part of the ridge shows a complex basement structure associated with short-wavelength magnetic anomalies (Goslin et al., 1980), whereas the southern part has a much more subdued topography with an extensive area of uniform sedimentation (Goslin et al., 1981). The Moho depth has been estimated to be 22–26 km in the transition zone at 31°S and to be 14 km in the southern part (Goslin et al., 1981; Schlich, 1982). Assuming a crustal density between 2,470 and 2,670 kg/m^3, the crust has been estimated to be 14-km thick according to the gravity model (Goslin et al., 1981). Suo et al. (2016) proposed a thick oceanic crust here on the basis of the low residual mantle Bouguer anomaly (RMBA) around the northern and southern parts of the Madagascar Ridge. The crustal thickness varies from north to south. The transition zone has an intermediate structure between normal oceanic and continental crust, and the southern part clearly has the structure of oceanic crust (Schlich, 1982). However, the age and nature of the ridge remain in question because no basement samples of the Madagascar Ridge have been recovered by deep-sea drilling at sites 246 and 247 (Schlich et al., 1974).

The Del Cano Rise is a composite feature trending in the east-west direction and lies south of the SWIR at ~45°–48°E (Figure 1). This rise has a smooth topography that culminates at a depth of ~1,500 m. The overall structure and sedimentary cover are quite similar to those of the southern Madagascar Ridge. Both bathymetric highs show uniform sedimentation across an extended area (Schlich, 1982). The Del Cano Rise has been estimated to have a 16-km thick oceanic crust with a crustal density of 2,600 kg/m^3 on the basis of mechanical and thermal isostatic responses (Goslin & Diament, 1987). This is similar to the southern Madagascar Ridge, which has been estimated to have a 14-km thick oceanic crust. A low RMBA has also been estimated for the rise (Suo et al., 2016). Based on the symmetric magnetic anomalies south of the southern Madagascar Ridge and north of the Crozet Plateau, the Madagascar Ridge and part of the Del Cano Rise probably have a common origin and later separated following the early Paleocene (Goslin et al., 1981). The Del Cano Rise has been proposed to have originated from anomalous volcanism caused by a significant change in the relative plate motion or spreading rate/direction of the young lithosphere near the active SWIR based on local Airy compensation of its topography (Goslin & Diament, 1987). Zhang et al. (2011) incorporated this gravity signature with the global plate model to propose that the Del Cano Rise formed when the Marion hotspot was close to the SWIR. Although the Del Cano Rise has been recognized as having thick oceanic crust by various geophysical features, no rock samples have been recovered, so the nature of this rise remains in question, similar to that of the southern Madagascar Ridge. In addition, as mentioned in Section 1, previous magnetic surveys were mostly not aligned to the spreading direction (Figure 2a), causing difficulty in age identification. Currently, seafloor age identifications have increased compared with those of the early 1980s (Figure 2b), but the majority of them are in the off-axis areas of the IG segment, whereas the southern Madagascar Ridge and the Del Cano Rise are emplaced in the DI segment (Figure 1), which has fewer identifications. Overall, the detailed seafloor spreading history between the two rises remains unknown.

3. Materials and Methods

Magnetic data across the SWIR were acquired in December 2009, December 2010–January 2011, February 2016, and January 2019 during cruises of the *R/V Hakuho-Maru* (KH-09-5, KH-10-7, KH-16-1, and KH-19-1, respectively). The survey lines were generally parallel to the predicted seafloor spreading direction (Figure 2a). We also used magnetic data acquired during a cruise of *R/V Marion Dufresne* (Magofond4 Leg2) and personal data provided by Professor J. Dyment. Open-source geomagnetic data from the National Geophysical Data Center (https://www.ngdc.noaa.gov) and several restricted sources of geomagnetic data (MD150 (Roest, 2005) and MD165 (Vially et al., 2008) cruises) provided by French oceanographic cruises (https://www.flotteoceanographique.fr) were also used.

3.1. Geomagnetism

We used two types of magnetometers: a surface-towed proton precession magnetometer and a shipboard three-component magnetometer.

3.2. Derivation of the Total Magnetic Field

The total magnetic field intensity was acquired every 30 s by using a surface-towed proton precession magnetometer (PR-745, Kawasaki Geological Engineering Co., Ltd.). The sensor was towed ∼300 m behind the vessel to reduce the magnetic effects of the ship. Magnetic anomalies were calculated by subtracting the 12th generation of the International Geomagnetic Reference Field (Thébault et al., 2015) from the observed magnetic field intensity. No crossover correction was applied because of the few crossover data points. For seafloor age identification, we calculated the equivalent crustal magnetization by using the two-dimensional (2D) inversion method of Parker and Huestis (1974) on the bathymetric profiles for several survey lines in the DI and GI segments. Both our new data and several previous data sets were used in this calculation. The direction of seafloor magnetization was postulated to be the same as that of the geocentric axial dipole field. We chose the midpoint of each magnetic profile to calculate the geocentric axial dipole field direction. Prior to the calculation, several magnetic tracks that were somewhat winding were fitted to the best-fit great circle. The mean geocentric axial dipole field was 42.8° ± 5.4°S (mean value ± standard deviation), which corresponds to $I = -61.5° \pm 0.6°$. We assumed a 500-m-thick magnetized layer, and we did not consider the sediment thickness. A bandpass filter with cutoff wavelengths of 5 and 120 km was applied to each iteration to stabilize the solution. The calculated magnetization patterns (normal and reversed) were roughly balanced, so we did not add an annihilator. The identified isochrons are plotted in Figures 3 and 4. We note that a few isochrons are not on the magnetic survey lines because the isochron positions are identified based on the great circle-fitted profiles. These offsets are small enough not to affect our interpretation. We identified the seafloor ages at other segments from the shapes of the magnetic anomalies. We also used 2D forward magnetic model software MODMAG (Mendel et al., 2005) to compare the synthetic and observed magnetic anomalies (Figures 3b and S3). We used these equivalent magnetization profiles with the geomagnetic polarity reversal time scale of Ogg (2012) to calculate the seafloor spreading rates for the DI and IG segments.

3.3. Acquisition of the Vector Magnetic Field

The primary advantage of vector measurement is for determining the location and strikes of magnetic boundaries from a single survey line (Seama et al., 1993). Thus, it is suitable for such a vast and low-accessibility area. We obtained vector magnetic field data by using a shipborne fluxgate magnetometer. The sampling interval was 0.125 s during the KH-16-1 cruise and 1 s during the KH-10-7 cruise. Coordinate axes extended longitudinally along the ship, across the ship, and vertically. We acquired the vessel attitude data by using a vessel-equipped gyrocompass. The observed vector magnetic data were affected by the motion and magnetization of the vessel; to remove these effects, we calculated a set of coefficients for ship magnetization by using the least squares method (Isezaki, 1986; Korenaga, 1995; Seama et al., 1993) and the data acquired as the vessel performed a figure-eight turn. Because of the limited roll and pitch ranges, we improved the vertical components of the coefficient by combining all figure-eight turn data from different latitudes. We calculated vector magnetic anomalies in the north, east, and vertical directions by subtracting the 12th generation of the International Geomagnetic Reference Field (Thébault et al., 2015) from the corrected magnetic field data. We applied a 20 s low-pass filter and 0.5–1.5 km

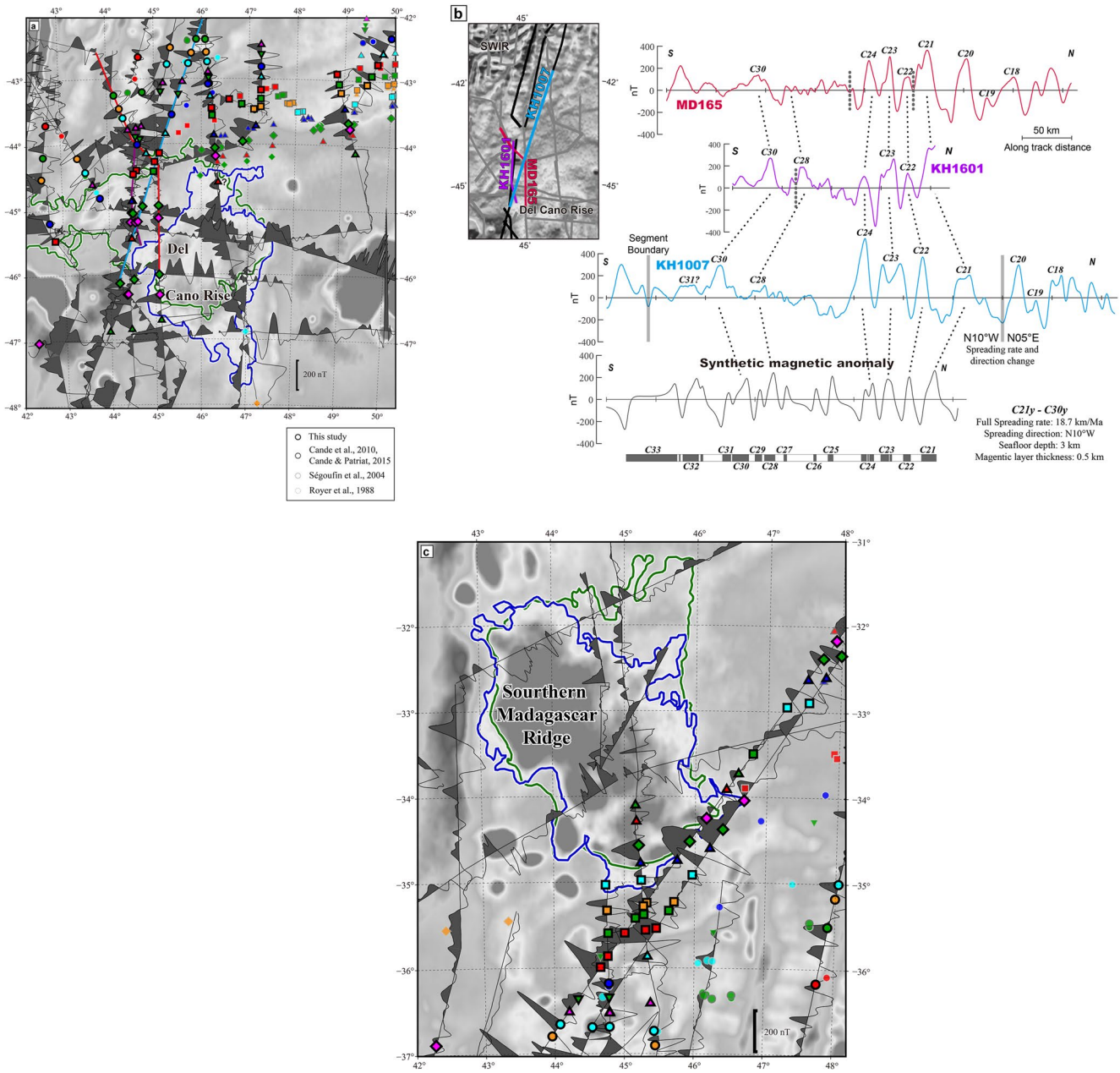

Figure 3. (a) Magnetic anomaly map around the Del Cano Rise. Newly and previously interpreted isochrons are plotted over magnetic anomaly profiles. The background image indicates the satellite-based free-air gravity anomaly, as shown in Figure 1. The thick cyan, purple, and red lines correspond to the magnetic survey lines in Figure 3b. (b) Magnetic anomaly profiles between the SWIR and Del Cano Rise. The vertical dotted gray lines indicate waypoints of the track lines. The horizontal axis represents the track line distance. The bottom part shows a synthetic magnetic anomaly between Chrons 33 and 21. (c) Magnetic anomaly map around the southern Madagascar Ridge.

cosine-tapered low-pass filter to remove the periodic effects of roll and pitch. A linear trend, which we assumed to be related to the time-dependent variation in the vessel's magnetization, was also subtracted from the magnetic anomalies. The correlation between the magnetic anomalies derived from the proton precession magnetometer data and the vector magnetic anomalies showed sufficient consistency to confirm their variations (Figure S5). We used the intensity of the spatial differential vector (ISDV) method (Seama et al., 1993) to calculate magnetic boundaries from the three-component magnetic anomalies. ISDVs reach maxima at magnetic boundaries regardless of the magnetization direction. We used STCMkit (Korenaga, 1995) to analyze the data and calculated magnetic boundary strike diagrams (MBSDs) at each ISDV peak location.

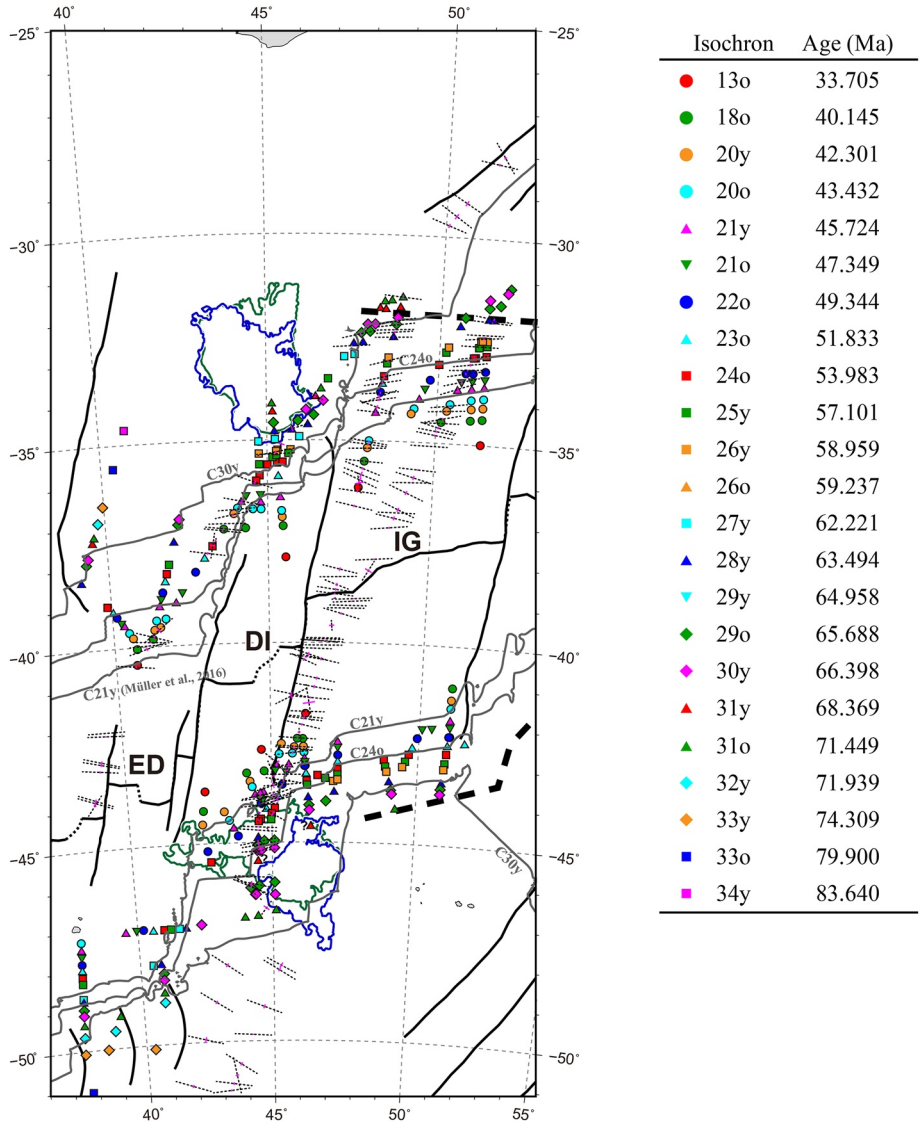

Figure 4. Newly interpreted isochrons in the survey area using the geomagnetic polarity reversal time scale of Ogg (2012). Other previous data are also plotted. The thin gray lines indicate the seafloor ages of Chron 21 (45.7–47.4 Ma) and Chron 30 (66.4–68.2 Ma) extracted from the global age model (Müller et al., 2016). Magnetic boundary strike diagrams (MBSDs) are also overlain. The dashed black lines indicate the azimuths of the strikes, and the lengths indicate the cosine of the inclination. The thin purple lines indicate the angular standard deviation, and longer lines indicate larger standard deviations.

3.4. Identification of the Seafloor Age

We identified the seafloor ages between the DI and IG segments in the survey area on the basis of magnetic isochrons from Chron 31o (69.3 Ma) to Chron 1 (0 Ma). In this study, we focused on the period between Chron 30y (66.4 Ma) and Chron 21y (45.7 Ma) and used the geomagnetic polarity reversal time scale of Ogg (2012) (Figures 2b and 4). Figure 4 shows the newly identified magnetic isochrons (Cande & Patriat, 2015; Cande et al., 2010; Royer et al., 1988; Ségoufin et al., 2004) and MBSDs along with the seafloor age model of Müller et al. (2016). The seafloor age identifications, including the previous results, are shown in Figure S2.

4. Results

4.1. Southern DI and IG Segments

We identified Chrons 28y, 29o, 30y, and 31y for the seafloor northwest of the Del Cano Rise at ~45°20′S, 45°E (Figures 3 and 4). Figure 3b shows examples of the magnetic anomaly profiles. Several magnetic anomalies have single peaks in the synthetic profile with doublets in the data (e.g., Chron 23) and vice versa (Chron 24). Although some observed magnetic profiles are not fitted for the synthetic profiles, we consider that our identified isochrons are reasonable because the isochrons were continuously identified in an orderly manner starting from the younger ages (e.g., Chrons 1, 13, and 18) (Figures 3b and S3). We also identified Chrons 29o, 30y, and 31y at 46°30′S, 44°E, which indicates that there may be a left-lateral offset ~100-km long on the western side of the Del Cano Rise. Along the southern off-axis region of the IG segment, we identified Chrons 30y and 31o from west to east, which indicates a left-lateral offset ~100-km long between the DI and IG segments during that period (Figures 3a and 4). In the IG segment, Chrons 24 and 30 are nearly parallel to each other, and we identified no age offset within the entire length of the IG segment. We did not identify Chron 32 (71.4–74.0 Ma) or older isochrons in the southern off-axis region of these two segments. We identified only Chrons 28o, 30y, and 31y at the rim of the rise. However, we did not observe magnetic anomalies that fit the geomagnetic polarity reversal model in the central part of the rise (Figures 3a and 4).

4.2. Northern DI and IG Segments

The northern off-axis area of the IG segment showed well-ordered magnetic anomaly reversal patterns, and the oldest identified isochron was Chron 31o (Figures 3c and 4). We also identified magnetic reversal patterns in the northern off-axis area of the DI segment, and the oldest isochron was Chron 31o. This indicates an ~200 km offset between the DI and IG segments based on the isochron patterns of the two segments. However, the position and details of the offset are unclear because of the lack of magnetic data around the boundary. The seafloor isochrons from Chron 21y to Chron 31o in the northern IG segment are well-ordered and nearly parallel to each other, which is similar to the conjugate area of the IG segment (Figures 3c, 4, and S3). In the northeastern most part of the IG segment, the oldest identified isochron is Chron 28y, which abuts the Madagascar Basin.

4.3. Seafloor Age Difference Between Models

In the off-axis area of the IG segment, Royer et al. (1988), Ségoufin et al. (2004), and Cande et al. (2010) identified isochrons up to Chron 29o, whereas Cande and Patriat (2015) identified isochrons up to Chron 31o. Our estimated positions for Chron 30y or younger are nearly the same as those for the other proposed seafloor age models (Figures 3a, 3c, and S2). The positions of Chron 31y and older differ somewhat among studies. For example, some of the anomalies in the off-axis areas of the IG segment that we identified as Chron 30y were identified as Chron 31y by Cande and Patriat (2015). Both sides of the off-axis areas of the DI segment had very few previously identified isochrons compared with the IG segment. The oldest identified isochrons were Chrons 24o and 20o for the northern and southern off-axis areas, respectively (Cande et al., 2010; Royer et al., 1988; Ségoufin et al., 2004). On the basis of our results, we were able to add extensive new isochrons in the DI segment. Isochrons younger than Chron 24o were mostly similar to the previous data (Figures 3a, 3c, and S2). For seafloor areas older than Chron 24o, no isochrons had been identified in previous studies, so we compared our results with the global age model (Müller et al., 2016; Figures 4 and S2). We identified Chron 30y with errors of ~100 km in the northern off-axis area and ~100–200 km in the southern off-axis area when compared with the global age model (Figures 3 and 4). As the global age model is constructed by referring to the isochrons, this discrepancy could be attributed to the sparse coverage of magnetic data/isochrons in the off-axis areas of the DI segment (Figure 2).

We identified magnetic isochrons up to Chron 31o by combining the previous data with our newly obtained data in the DI and IG segments, although there was uncertainty regarding Chrons 31y and 31o (Figures 3, 4, and S3). However, previous studies have not identified Chron 32 and older in the off-axis areas of both the DI and IG segments, including the southern Madagascar Ridge and Del Cano Rise (Cande & Patriat, 2015; Cande et al., 2010; Royer et al., 1988; Ségoufin et al., 2004; Figures 3 and 4). According to the global magnetic anomaly model (EMAG2, Maus et al., 2009), the magnetic anomalies observed for these two rises did not show any magnetic reversal patterns implying a seafloor spreading process. Thus, we suggest that the seafloor farther north and

south of Chron 31o across these two segments did not form by spreading of the SWIR. However, we cannot rule out the possibility that sporadic magmatic activity may have obscured the preexisting magnetic reversal patterns.

4.4. Spreading Rate and Direction

For isochrons younger than Chron 30, we calculated the spreading rate by using magnetic data (Table S1). Between Chrons 30 and 21, the full spreading rates of the DI and IG segments were 17.6 and 18.6 km/Ma, respectively, which can be classified as ultraslow. Spreading asymmetry was observed for both segments (Table S1). For the IG segment, we also calculated the spreading rate from Chron 20 to Chron 1 (SWIR spreading axis). The spreading rate was 25.4 km/Ma from Chron 20 to Chron 6, which can be classified as slow. This is similar to the spreading rate of 29 km/Ma that was calculated by Patriat et al. (2008), but our estimated rate is slightly lower. The spreading rate was calculated as 14.9 km/Ma between Chron 6 and the spreading axis, which is similar to the present SWIR spreading rate of 15 km/Ma (MORVEL; DeMets et al., 2010).

We estimated the spreading direction by using MBSDs from vector magnetic field data measured during our surveys. In the DI and IG segments, the azimuth of the MBSDs changed slightly at approximately Chron 21 (Figure 4). In the IG segment, the mean azimuth of MBSDs younger than Chron 21 was approximately N95°E, whereas that between Chrons 30 and 21 was approximately N82°E and was calculated in only the northern off-axis area (Figure S4). In the DI segment, the mean azimuth of the MBSDs was approximately N80°E in the southern off-axis area. The northern IG segment had little data, but the mean azimuth was calculated as N80°E, which is the same as that for the southern area. Considering that MBSDs with higher ISDVs (in this study, we chose a threshold of 40 nT/km for the ISDV) represent the direction of a magnetic boundary, the orthogonal direction of the MBSDs should be equal to the spreading direction. Therefore, a change in the spreading rate and direction would be expected at Chron 21.

5. Discussion

5.1. Model Reconstruction of the Middle SWIR From Chrons 30 to 21

On the basis of our identified isochrons, MBSDs, FZ flow lines, and several lineaments detected from gravity anomalies and the VGG (Figure S1), we reconstructed a model of seafloor spreading between the southern Madagascar Ridge and Del Cano Rise. We focused our model on Chrons 30, 24, and 21. We used visual fitting for the reconstruction because we were considering the spreading history of only two segments of the SWIR. We fixed the Antarctic Plate at its present position and moved the African Plate for the reconstruction. Figure 5a shows the reconstruction of Chron 30y (66.4 Ma). Our model indicated that the higher gravity areas of the southern Madagascar Ridge and Del Cano Rise (surrounded by thick blue lines) were adjacent to each other at this time. This idea had already been proposed (Goslin et al., 1980) but was based on sparse magnetic surveys. Isochron identifications are still sparse in the DI segment after several subsequent studies (Figure 2b). Our model revealed the detailed separation history between the two rises for the first time. Comparing the global age model (Müller et al., 2016) with our newly identified isochrons, remarkably, Chron 30y was located to the south of the Del Cano Rise in the former was identified to the north of the rise in the latter. Our model suggests that the Del Cano Rise already existed by Chron 30y. This is in sharp contrast with the global age model, which shows that the majority of the rise had not formed at that time.

We named the segments between these two rises T1, R1, and R2 from west to east (Figures 5a and 5b). The T1 segment was >200-km long and differed in direction from the other segments. The T1 segment was connected to the ED segment in the west and to the R1 segment in the east. The R1 and R2 segments were at least 100-km and 60-km long, respectively, based on our magnetic data. A left-lateral offset that was ∼100-km long bounded these two segments. The R2 segment was connected to the IG segment in the east by an offset, but the details are unclear. Ultraslow-spreading (18–19 km/Ma) trending N10°W started at the R1, R2, and IG segments at Chron 30 or Chron 31 and continued to Chron 21.

Figure 5b shows the reconstruction of Chron 24o (53.4 Ma). By this stage, the SWIR east of the Gallieni FZ had started to propagate eastward (Dyment, 1993). Additionally, significant changes have been suggested to have occurred in the migration path of the Africa-Antarctic stage pole at Chron 24o (Cande & Patriat, 2015). The ED, R1, and IG segments were identified. However, an offset observed at Chron 30y between the R1 and R2 segments

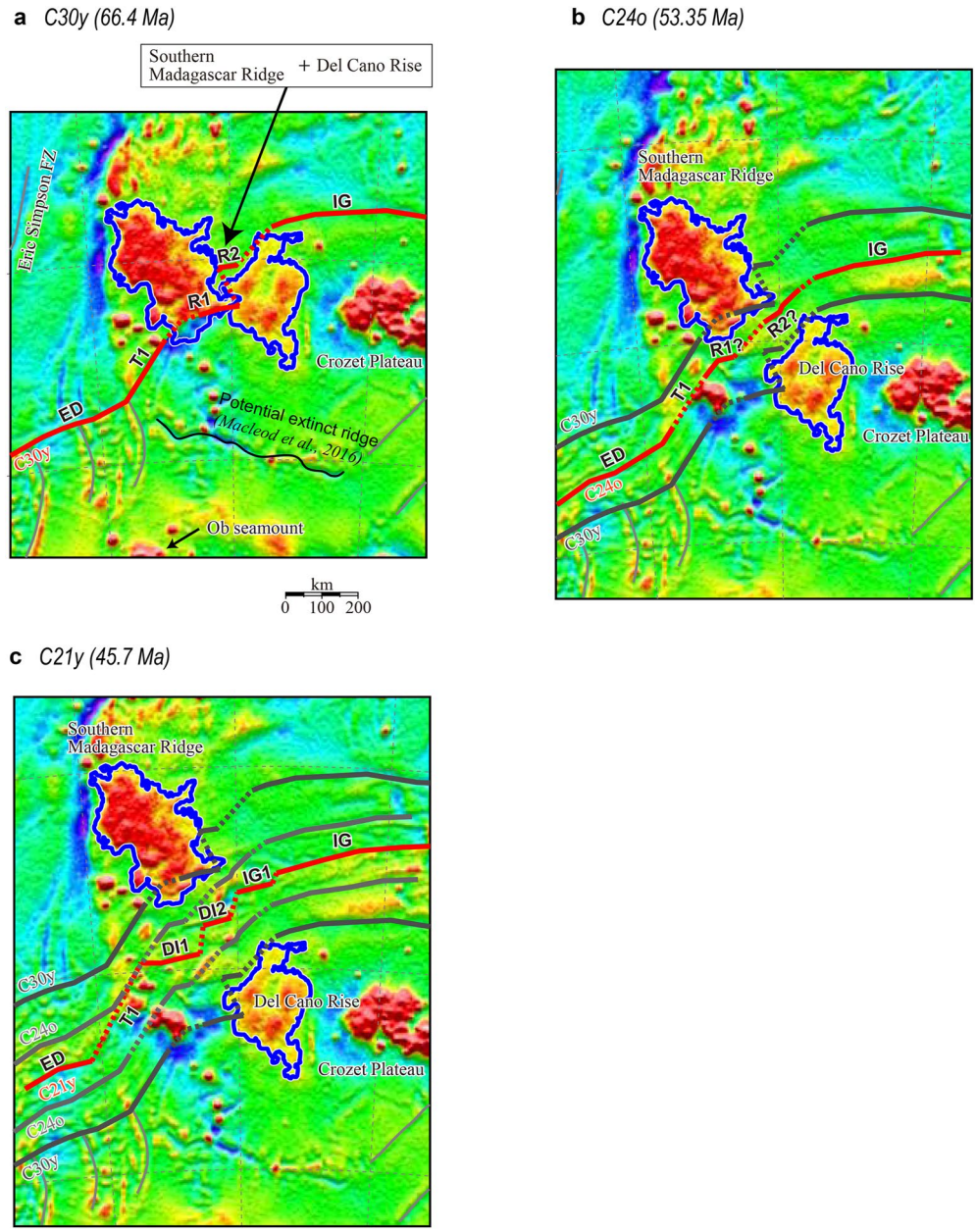

Figure 5. Reconstruction models of ages of Chrons (a) 30y, (b) 24o, and (c) 21y based on visual fitting. The background image was generated from satellite-based free-air gravity anomalies (Sandwell et al., 2014). The solid and dashed red lines indicate the spreading axis and discontinuities, respectively, at each reconstruction stage. The thick blue lines around the southern part of the Madagascar Plateau and Del Cano Rise indicate free-air gravity anomalies greater than 30 mGal.

seems to have become shorter or disappeared. Hence, the segmentation pattern differed from that at Chron 30y. This pattern could be observed at Chrons 25 and 26, so segment reorganization started at that age.

Figure 5c shows the reconstruction of Chron 21y (45.7 Ma). The segments had been reorganized, and three segments (DI1, DI2, and IG1) had developed with lengths of approximately 160, 70, and 100 km, respectively, in the west-east direction and bounded by left-lateral offsets. These segments may have evolved from parts of the T1, R1, and R2 segments. This segmentation pattern is similar to the present configuration of the spreading axis (Figure 1). Therefore, we infer that the DI1 and DI2 segments evolved into second-order segments of the DI segment. The IG1 segment evolved into a second-order segment of the IG segment (Figure 1). Part of the T1

segment may have transformed into the Discovery II FZ, and the offset between the DI2 and IG1 segments would have become the Indomed FZ.

5.2. Formation of the Southern Madagascar Ridge and Del Cano Rise

We propose that the southern Madagascar Ridge and Del Cano Rise were a single bathymetric high by at least Chron 30 (Figure 5a). These rises have been listed as oceanic LIPs (e.g., Bryan & Ernst, 2008; Coffin & Eldholm, 1994) with 14–16-km thick oceanic crust (Goslin & Diament, 1987; Goslin et al., 1981). The free-air anomalies vary from 30 to 90 mGal over the southern Madagascar Ridge and from 30 to 50 mGal over the Del Cano Rise; thus, the two rises are characterized by only positive gravity anomalies (Figures 2a and 5). Considering that the two rises are adjacent, their similar gravity features and crustal thicknesses suggest the same origin. Plume-ridge/triple junction interaction is one of the possible causes for thicker-than-normal oceanic crust, rather than LIP volcanism emplaced onto the preexisting oceanic crust (e.g., Jiang et al., 2021; Sager et al., 2019; Zhang et al., 2011). Excess volcanism around an active spreading ridge may produce a thick crust without plate flexure. For understanding whether this interaction is applicable to the two rises, it is essential to know the relative locations among plume, ridge, and triple junction when the interaction occurred. Hence, plume-ridge/triple junction interaction at the southwestern Indian Ocean has been discussed (Desa et al., 2019; Georgen et al., 2001; Homrighausen et al., 2021; Zhang et al., 2011); however, the relative locations are different in each model because they depend on the plate motion model and hotspot model used. For example, Desa et al. (2019) suggested that the Marion hotspot was located east of the northern Madagascar Ridge and that the triple junction was located at the eastern end of the IG segment at Chron 31y (67.7 Ma) (Figure 8 in Desa et al., 2019). On the other hand, Homrighausen et al. (2021) proposed that the Marion hotspot was located near a triple junction at 75 Ma (during Chron 33n) and located in the Antarctic plate at 65 Ma (during Chron 29n) (Figure 10 in Homrighausen et al., 2021). Therefore, the relative locations of plume, ridge, and triple junction at the separation stage of the southern Madagascar Ridge and the Del Cano Rise remain unclear, so it seems difficult to discuss the plume-induced ridge/triple junction dynamics from their relative locations. For this reason, we discuss the origin of the two rises in terms of magnetic and gravity features.

In research on excess volcanism in oceanic LIPs coupled with mid-ocean ridges, the Tamu Massif has recently been recognized as having formed from voluminous and focused ridge volcanism rather than as a shield volcano (Sager et al., 2019). The magmatic activity is controlled by seafloor spreading so that linear magnetic anomalies are observed on the massif (Sager et al., 2019). If the southern Madagascar Ridge and the Del Cano Rise were also formed by plume-ridge interaction, linear magnetic anomalies should be observed on the massifs. The continuity of the seafloor age identifications from the spreading axis of the SWIR suggests that the two rises had formed before Chron 31; however, no isochrons with older ages and no linear magnetic anomalies were observed (Figures 3a and 3c) in our study. The preexisting isochrons (Cande & Patriat, 2015; Cande et al., 2010; Royer et al., 1988; Ségoufin et al., 2004) have also not been interpreted for these rises (Figures 3a, 3c, and S2). In addition, linear magnetic anomalies cannot be seen in the global magnetic anomaly model (EMAG2; Maus et al., 2009). Thus, the observed magnetic characteristics imply that seafloor spreading of the SWIR may not have controlled the formation of the main parts of these two rises.

The formation age of the southern Madagascar Ridge and the Del Cano Rise may be older because an extinct ridge has been predicted between the Del Cano Rise and Conrad Rise (MacLeod et al., 2017). Based on the preexisting isochrons (Ségoufin et al., 2004), ridge activity was presumed to cease at approximately Chron 33o. Chron 34y is also identified north of the Conrad rise, suggesting that the Del Cano Rise and the southern Madagascar Ridge had formed before then. In addition, the extinct ridge implies that a northward ridge jump occurred to the SWIR. The assumption of an extinct ridge corresponds to the fact that the identified oldest isochron was Chron 31o in the DI and IG segments of the SWIR. Due to the ridge jump, the Del Cano Rise may have been transferred from the African Plate to the Antarctic Plate.

For the origin of thick crust, especially for the Del Cano Rise, that is in a local isostatic state (Goslin & Diament, 1987), the rise has been proposed to have originated from excess volcanism emplaced on or near the active axis of the SWIR by a major change in the relative motions of the Antarctic and African Plates (Goslin & Diament, 1987). However, their proposed idea does not explain the thick crust of the rise. They suggested that either the change in spreading geometry began at Chron 28 or that the drastic reduction in the spreading rate around Chron 24 resulted in excess volcanism. However, such changes were not observed in this study, and the two

bathymetric highs had already separated by that time (Figure 5b). In addition, as we already mentioned, Marion hotspot-SWIR interaction can explain the thick crust and gravity signature of the Del Cano Rise and the southern Madagascar Ridge (e.g., Georgen et al., 2001; Zhang et al., 2011); however, our obtained magnetic features do not support a contribution from seafloor spreading to the formation of the main part of the Del Cano Rise. Moreover, plume-induced excess volcanism around the extinct ridge may also be ruled out because the plume was far from the ridge, although the triple junction was located east of the ridge around Chron 34y (Desa et al., 2019; Homrighausen et al., 2021). Therefore, different possibilities should be discussed for their origin other than plume-ridge/triple junction interaction.

There is a possibility that LIP volcanism was emplaced onto the preexisting oceanic crust. This process is difficult to discuss due to the lack of basement rock sampling and age constraints on these rises. However, if the rises had been caused by intraplate volcanism, a high gravity anomaly surrounded by a low gravity anomaly would be observed, which could be explained by plate flexure due to excess material loading on the oceanic lithosphere as for the Hawaiian shield volcanoes. However, the gravity signatures of these two rises are characterized by only high gravity anomalies, implying that intraplate volcanism is unlikely for their origin. Conversely, the Crozet Plateau is another oceanic LIP with an estimated crustal thickness of 10–16.5 km (Recq et al., 1998), which is similar to those of the southern Madagascar Ridge and Del Cano Rise, but the Crozet Plateau shows gravity features that can be explained by excess volcanism on preexisting oceanic crust. This also suggests that the southern Madagascar Ridge and the Del Cano Rise differ in origin from the Crozet Plateau.

Regarding other oceanic LIPs, the free-air gravity anomalies, crustal thickness, and magnetic anomalies of the Mozambique Ridge off southeastern Africa are similar to those of the southern Madagascar Ridge and Del Cano Rise. This ridge has free-air gravity anomalies from 30 to 70 mGal (Sandwell et al., 2014) with a crustal thickness of ~22 km (assuming a crustal density of 2,900 kg/m^3) and is in isostatic equilibrium (Hales & Nation, 1973). The magnetic anomalies do not show a reversal pattern (König & Jokat, 2010). On the basis of geophysical features, König and Jokat (2010) proposed that the Mozambique Ridge may be of oceanic origin and may have evolved in a region of high volcanic activity since the early beginning of the Gondwana breakup. The observed magnetic anomalies of the Mozambique Ridge can also be explained by massive basaltic extrusions/intrusions, dikes, and conduits that were emplaced at different times of normal and reversed magnetic polarities. However, these authors did not exclude the possibility that small continental fragments may exist near the Mozambique Ridge because several dredged samples showed continental affinity (e.g., Hartnady et al., 1992). In fact, continental fragments are recognized in the Indian Ocean. They are considered to have been emplaced/isolated during the breakup of Gondwana (e.g., the Elan Bank (Borissova et al., 2003), Naturaliste Plateau (Halpin et al., 2008), Laxmi Ridge (Naini & Talwani, 1982; Talwani & Reif, 1998), and Seychelles Plateau (Besse & Courtillot, 1988; Lawver & Gahagan, 1998)). Recently, Jiang et al. (2021) proposed that the Elan Bank and the southern Kerguelen Plateau were formed by plume-induced excess volcanism on continental lithosphere (Figure 4 in Jiang et al., 2021).

We propose that the southern Madagascar Ridge and the Del Cano Rise may have been formed partly by continental fragments. These two rises have been recognized as oceanic LIPs; however, the observed magnetic anomalies and isochrons suggest that plume-induced excess volcanism controlled by seafloor spreading can be ruled out for their main origin. The magnetic anomalies can also be explained by sporadic magmatic activity similar to that of the Mozambique Ridge. The thicker-than-normal crust and low RMBAs of these rises may be explained by continental fragments covered by volcanic activity, similar to the model for the Elan Bank and the southern Kerguelen Plateau. Our hypothesis is based on the seafloor spreading history constructed from magnetic surveys, so additional geophysical surveys (gravity and seismic refraction/reflection) and direct geological evidence (rock samples) are essential to clarify the nature and origin of the rises.

6. Conclusions

Based on newly obtained magnetic data, we revised the seafloor ages in the central SWIR between the Discovery II and Indomed FZs in the Indian Ocean. We combined the identified seafloor ages on the basis of the total force magnetic anomalies, MBSDs calculated from three-component magnetic field anomalies, and open-source satellite-based gravity anomalies to reach the following conclusions:

(1) The oldest identified isochron was Chron 31o. Between Chrons 30y and 21y, the seafloor full spreading rate was ~18–19 km/Ma, which is classified as ultraslow and the same as the present spreading rate of the SWIR. The spreading direction was approximately N10°W (MBSD direction is N80°E) from Chron 30y to Chron 21y. Following Chron 21y, the spreading rate increased to ~25 km/Ma, and its direction changed to approximately N05°E (MBSD direction is N95°E)

(2) On the basis of our reconstruction of the seafloor spreading history, we propose that the southern Madagascar Ridge and Del Cano Rise once formed a single bathymetric high. The separation between the two would have occurred by Chron 30y. This is quite different from the global age model, which shows that most of the rise had not formed at that time. The segmentation pattern at Chron 30y differs from that of the present SWIR. The reorganization of the segments occurred around Chron 24, and the current segmentation pattern began around Chron 21. Our reconstruction suggests that the Discovery II and Indomed FZs did not exist when the southern Madagascar Ridge and Del Cano Rise separated but emerged around Chron 21

(3) Based on the magnetic features of the southern Madagascar Ridge and the Del Cano Rise, we propose that plume-induced excess volcanism controlled by seafloor spreading can be ruled out as the main origin of these rises. Seafloor age identification of the DI and IG segments and the cessation age of the extinct ridge suggests that the two bathymetric highs may have formed before Chron 34y. These two rises may be isolated structures that were separated by a ridge jump and SWIR spreading. We propose that continental fragments overlain by magmatic activity may also be a possible explanation for their origins rather than plume-induced excess volcanism

Data Availability Statement

Seafloor bathymetric data and magnetic data acquired during previous French cruises (MD150 and MD165) are included in the analyses. The magnetic data acquired during cruises of the *R/V Hakuho-Maru* (KH-09-5, KH-10-7, KH-16-1, and KH-19-1) are available online (10.6084/m9.figshare.12111048).

Acknowledgments
This work was supported by the JSPS KAKENHI Grant No. 18H01317. The authors declare no competing interests. We appreciate the officers and crew of *R/V Hakuho-Maru* for their professional support of the data acquisition. We are grateful to the KH-09-5 Leg 4, KH-10-7, KH-16-1, and KH-19-1 shipboard scientific parties for onboard collaboration and discussions. We are also grateful to the officers and crew of the *R/V Marion Dufresne* for their professional support of the data acquisition. We thank the Magofond4 Leg 2 shipboard scientific party for providing their magnetic data and Prof. J. Dyment for providing his magnetic data. We also thank Prof. Z.X. Li and members of the Earth Dynamics group at Curtin University for their helpful discussion during T.S.'s stay as an adjunct visitor in 2018–2019. We also appreciate our editor and reviewers for their constructive comments.

References

Amante, C., & Eakins, B. W. (2009). ETOPO1 1 arc-minute global relief model: Procedures, data sources and analysis. *NOAA Technical Memorandum NESDIS NGDC-24*. National Geophysical Data Center, NOAA. https://doi.org/10.7289/V5C8276M

Besse, J., & Courtillot, V. (1988). Paleogeographic maps of the continents bordering the Indian ocean since the early Jurassic. *Journal of Geophysical Research*, *93*(B10), 11791–11802. https://doi.org/10.1029/JB093iB10p11791

Borissova, I., Coffin, M. F., Charvis, P., & Operto, S. (2003). Structure and development of a microcontinent: Elan bank in the southern Indian Ocean. *Geochemistry, Geophysics, Geosystems*, *4*(9), 1071. https://doi.org/10.1029/2003GC000535

Bryan, S. E., & Ernst, R. E. (2008). Revised definition of large igneous provinces (LIPs). *Earth-Science Reviews*, *86*(1–4), 175–202. https://doi.org/10.1016/j.earscirev.2007.08.008

Cande, S. C., & Patriat, P. (2015). The anticorrelated velocities of Africa and India in the late Cretaceous and early Cenozoic. *Geophysical Journal International*, *200*(1), 227–243. https://doi.org/10.1093/gji/ggu392

Cande, S. C., Patriat, P., & Dyment, J. (2010). Motion between the Indian, Antarctic and African plates in the early Cenozoic. *Geophysical Journal International*, *183*(1), 127–149. https://doi.org/10.1111/j.1365-246X.2010.04737.x

Coffin, M. F., & Eldholm, O. (1994). Large igneous provinces: Crustal structure, dimensions, and external consequences. *Reviews of Geophysics*, *32*(1), 1–36. https://doi.org/10.1029/93RG02508

DeMets, C., Gordon, R. G., & Argus, D. F. (2010). Geologically current plate motions. *Geophysical Journal International*, *181*(1), 1–80. https://doi.org/10.1111/j.1365-246X.2009.04491.x

Desa, M. A., Ramprasad, T., & Kamesh Raju, K. A. (2019). An integrated geophysical study east of the southern Chagos Laccadive ridge complex, central Indian Ocean basin: Implications for the Rodriguez triple junction dynamics in the late Cretaceous. *Marine Geology*, *414*, 47–63. https://doi.org/10.1016/j.margeo.2019.05.007

Dyment, J. (1993). Evolution of the Indian Ocean triple junction between 65 and 49 Ma (anomalies 28 to 21). *Journal of Geophysical Research*, *98*(B8), 13863–13877. https://doi.org/10.1029/93JB00438

Georgen, J. E., Lin, J., & Dick, H. J. B. (2001). Evidence from gravity anomalies for interactions of the Marion and Bouvet hotspots with the Southwest Indian Ridge: Effects of transform offsets. *Earth and Planetary Science Letters*, *187*(3–4), 283–300. https://doi.org/10.1016/S0012-821X(01)00293-X

Goslin, J., & Diament, M. (1987). Mechanical and thermal isostatic response of the Del Cano Rise and Crozet bank (southern Indian Ocean) from altimetry data. *Earth and Planetary Science Letters*, *84*(2–3), 285–294. https://doi.org/10.1016/0012-821X(87)90093-8

Goslin, J., Recq, M., & Schlich, R. (1981). Structure profonde du plateau de Madagascar: Relations avec le plateau de Crozet. *Tectonophysics*, *76*(1–2), 75–97. https://doi.org/10.1016/0040-1951(81)90254-7

Goslin, J., Ségoufin, J., Schlich, R., & Fisher, R. L. (1980). Submarine topography and shallow structure of the Madagascar Ridge, western Indian Ocean. *Geological Society of America Bulletin*, *91*(12), 741–753. https://doi.org/10.1130/0016-7606(1980)91<741:stasso>2.0.co;2

Hales, A. L., & Nation, J. B. (1973). A seismic refraction study in the southern Indian Ocean. *Bulletin of the Seismological Society of America*, *63*(6–1), 1951–1966. https://doi.org/10.1785/BSSA0636-11951

Halpin, J. A., Crawford, A. J., Direen, N. G., Coffin, M. F., Forbes, C. J., & Borissova, I. (2008). Naturaliste Plateau, offshore western Australia: A submarine window into Gondwana assembly and breakup. *Geology*, *36*(10), 807. https://doi.org/10.1130/G25059A.1

Hartnady, C. J. H., Ben-Avraham, Z., & Rogers, J. (1992). Deep-ocean basins and submarines rises off the continental margin of south-eastern Africa: New geological research. *South African Journal of Science*, *88*(11–12), 534–539. Retrieved from https://journals.co.za/doi/abs/10.10520/AJA00382353_9897

Homrighausen, S., Hoernle, K., Wartho, J. A., Hauff, F., & Werner, R. (2021). Do the 85°E Ridge and Conrad rise form a hotspot track crossing the Indian ocean? *Lithos*, *398–399*, 106234. https://doi.org/10.1016/j.lithos.2021.106234

Hosford, A., Tivey, M. A., Matsumoto, T., Dick, H. J. B., Schouten, H., & Kinoshita, H. (2003). Crustal magnetization and accretion at the Southwest Indian Ridge near the Atlantis II fracture zone, 0-25 Ma. *Journal of Geophysical Research*, *108*(B3), 2169. https://doi.org/10.1029/2001JB000604

Isezaki, N. (1986). A new shipboard three-component magnetometer. *Geophysics*, *51*(10), 1992–1998. https://doi.org/10.1190/1.1442054

Jiang, Q., Jourdan, F., Olierook, H. K. H., Merle, R. E., & Whittaker, J. M. (2021). Longest continuously erupting large igneous province driven by plume-ridge interaction. *Geology*, *49*(2), 206–210. https://doi.org/10.1130/G47850.1

König, M., & Jokat, W. (2010). Advanced insights into magmatism and volcanism of the Mozambique Ridge and Mozambique Basin in the view of new potential field data. *Geophysical Journal International*, *180*(1), 158–180. https://doi.org/10.1111/j.1365-246X.2009.04433.x

Korenaga, J. (1995). Comprehensive analysis of marine magnetic vector anomalies. *Journal of Geophysical Research*, *100*(B1), 365–378. https://doi.org/10.1029/94JB02596

Lawver, L., & Gahagan, L. (1998). A tight fit-early mesozoic Gondwana, a plate reconstruction perspective. *Memoirs of National Institute of Polar Research*, *53*, 214–229. Retrieved from https://ci.nii.ac.jp/naid/110000010427/ja/

MacLeod, S. J., Williams, S. E., Matthews, K. J., Müller, R. D., & Qin, X. (2017). A global review and digital database of large-scale extinct spreading centers. *Geosphere*, *13*(3), 911–949. https://doi.org/10.1130/GES01379.1

Maus, S., Barckhausen, U., Berkenbosch, H., Bournas, N., Brozena, J., Childers, V., et al. (2009). EMAG2: A 2-arc min resolution Earth magnetic anomaly grid compiled from satellite, airborne, and marine magnetic measurements. *Geochemistry, Geophysics, Geosystems*, *10*, Q08005. https://doi.org/10.1029/2009GC002471

Mendel, V., Munschy, M., & Sauter, D. (2005). MODMAG, a MATLAB program to model marine magnetic anomalies. *Computers & Geosciences*, *31*(5), 589–597. https://doi.org/10.1016/j.cageo.2004.11.007

Mendel, V., Sauter, D., Rommevaux-Jestin, C., Philippe, P., Lefebvre, F., & Parson, L. M. (2003). Magmato-tectonic cyclicity at the ultra-slow spreading Southwest Indian Ridge: Evidence from variations of axial volcanic ridge morphology and abyssal hills pattern. *Geochemistry, Geophysics, Geosystems*, *4*(5), 9102. https://doi.org/10.1029/2002GC000417

Müller, R. D., Seton, M., Zahirovic, S., Williams, S. E., Matthews, K. J., Wright, N. M., et al. (2016). Ocean basin evolution and global-scale plate reorganization events since pangea breakup. *Annual Review of Earth and Planetary Sciences*, *44*(1), 107–138. https://doi.org/10.1146/annurev-earth-060115-012211

Naini, B. R., & Talwani, M. (1982). Structural framework and the evolutionary history of the continental margin of western India. In J. S. Watkins, & C. L. Drake (Eds.), *Studies in continental margin geology* (pp. 167–191). American Association of Petroleum Geologists. https://doi.org/10.1306/M34430C9

Niu, X., Ruan, A., Li, J., Minshull, T. A., Sauter, D., Wu, Z., et al. (2015). Along-axis variation in crustal thickness at the ultraslow spreading Southwest Indian Ridge (50°E) from a wide-angle seismic experiment. *Geochemistry, Geophysics, Geosystems*, *16*, 468–485. https://doi.org/10.1002/2014GC005645

Norton, I. O., & Sclater, J. G. (1979). A model for the evolution of the Indian Ocean and the breakup of Gondwanaland. *Journal of Geophysical Research*, *84*(B12), 6803–6830. https://doi.org/10.1029/JB084iB12p06803

Ogg, J. G. (2012). Geomagnetic polarity time scale. In F. M. Gradstein, J. G. Ogg, M. D. Schmitz, & G. M. Ogg (Eds.), *The geologic time scale* (Vol.1–2, pp. 85–113). Elsevier. https://doi.org/10.1016/B978-0-444-59425-9.00005-6

Parker, R. L., & Huestis, S. P. (1974). The inversion of magnetic anomalies in the presence of topography. *Journal of Geophysical Research*, *79*(11), 1587–1593. https://doi.org/10.1029/JB079i011p01587

Patriat, P., & Ségoufin, J. (1988). Reconstruction of the central Indian ocean. *Tectonophysics*, *155*(1–4), 211–234. https://doi.org/10.1016/0040-1951(88)90267-3

Patriat, P., Sloan, H., & Sauter, D. (2008). From slow to ultraslow: A previously undetected event at the Southwest Indian Ridge at ca. 24 Ma. *Geology*, *36*(3), 207–210. https://doi.org/10.1130/G24270A.1

Recq, M., Goslin, J., Charvis, P., & Operto, S. (1998). Small-scale crustal variability within an intraplate structure: The Crozet bank (southern Indian Ocean). *Geophysical Journal International*, *134*(1), 145–156. https://doi.org/10.1046/j.1365-246X.1998.00530.x

Roest, W. R. (2005). MD 150/DELCANO RISE-KERGUEPLAC2 cruise. *RV Marion Dufresne*. https://doi.org/10.17600/5200060

Royer, J.-Y., Patriat, P., Bergh, H. W., & Scotese, C. R. (1988). Evolution of the Southwest Indian Ridge from the late Cretaceous (anomaly 34) to the middle Eocene (anomaly 20). *Tectonophysics*, *155*(1–4), 235–260. https://doi.org/10.1016/0040-1951(88)90268-5

Royer, J.-Y., & Sandwell, D. T. (1989). Evolution of the eastern Indian ocean since the late Cretaceous: Constraints from Geosat altimetry. *Journal of Geophysical Research*, *94*(B10), 13755–13782. https://doi.org/10.1029/JB094iB10p13755

Sager, W. W., Huang, Y., Tominaga, M., Greene, J. A., Nakanishi, M., & Zhang, J. (2019). Oceanic plateau formation by seafloor spreading implied by Tamu Massif magnetic anomalies. *Nature Geoscience*, *12*(8), 661–666. https://doi.org/10.1038/s41561-019-0390-y

Sandwell, D. T., Müller, R. D., Smith, W. H. F., Garcia, E., & Francis, R. (2014). New global marine gravity model from CryoSat-2 and Jason-1 reveals buried tectonic structure. *Science*, *346*(6205), 65–67. https://doi.org/10.1126/science.1258213

Sauter, D., Cannat, M., Meyzen, C. M., Bezos, A., Patriat, P., Humler, E., & Debayle, E. (2009). Propagation of a melting anomaly along the ultraslow Southwest Indian Ridge between 46°E and 52°20′E: Interaction with the Crozet hotspot? *Geophysical Journal International*, *179*(2), 687–699. https://doi.org/10.1111/j.1365-246X.2009.04308.x

Sauter, D., Patriat, P., Rommevaux-Jestin, C., Cannat, M., & Briais, A. (2001). The Southwest Indian Ridge between 49°15′E and 57°E: Focused accretion and magma redistribution. *Earth and Planetary Science Letters*, *192*(3), 303–317. https://doi.org/10.1016/S0012-821X(01)00455-1

Schlich, R. (1982). The Indian Ocean: Aseismic ridges, spreading centers, and oceanic basins. In *The ocean basins and margins*. Springer US. https://doi.org/10.1007/978-1-4615-8038-6_2

Schlich, R., Simpson, E. S. W., Gieskes, J., Girdley, W. A., Leclaire, L., Marshall, B. V., et al. (1974). *Sites 246 and 247 initial reports of the Deep Sea Drilling Project, 25* (Vol. 25, pp. 237–257). U.S. Government Printing Office, Ocean Drilling Program. https://doi.org/10.2973/dsdp.proc.25.108.1974

Seama, N., Nogi, Y., & Isezaki, N. (1993). A new method for precise determination of the position and strike of magnetic boundaries using vector data of the geomagnetic anomaly field. *Geophysical Journal International*, *113*(1), 155–164. https://doi.org/10.1111/j.1365-246X.1993.tb02536.x

Ségoufin, J., Munschy, M., Bouysse, P., & Mendel, V. (2004). *Map of the Indian ocean, sheet 1: Physiography, sheet 2: Structural map, scale 1:20.000.00*. Commission for the Geological Map of the World. Retrieved from https://ccgm.org/en/home/210-map-of-the-indian-ocean-pdf-9782917310335.html

Suo, Y., Li, S., Li, X., Guo, L., & Wang, Y. (2016). Crustal thickness anomalies in the Indian Ocean inferred from gravity analysis. *Geological Journal*, *51*, 634–643. https://doi.org/10.1002/gj.2786

Talwani, M., & Reif, C. (1998). Laxmi Ridge—A continental sliver in the Arabian Sea. *Marine Geophysical Research*, *20*(4), 259–271. https://doi.org/10.1023/A:1004674909280

Thébault, E., Finlay, C. C., Beggan, C. D., Alken, P., Aubert, J., Barrois, O., et al. (2015). International geomagnetic reference field: The 12th generation. *Earth, Planets and Space*, *67*(1), 79. https://doi.org/10.1186/s40623-015-0228-9

Vially, R., Brunet, C., & Royer, J.-Y. (2008). *MD 165/KERGUEPLAC 3 cruise*. RV Marion Dufresne. https://doi.org/10.17600/8200010

Zahirovic, S., Müller, R. D., Seton, M., Flament, N., Gurnis, M., & Whittaker, J. (2012). Insights on the kinematics of the India-Eurasia collision from global geodynamic models. *Geochemistry, Geophysics, Geosystems*, *13*, Q04W11. https://doi.org/10.1029/2011GC003883

Zhang, T., Lin, J., & Gao, J. Y. (2011). Interactions between hotspots and the Southwest Indian Ridge during the last 90 Ma: Implications on the formation of oceanic plateaus and intra-plate seamounts. *Science China Earth Sciences*, *54*(8), 1177–1188. https://doi.org/10.1007/s11430-011-4219-9

Zhang, T., Lin, J., & Gao, J. Y. (2013). Magmatism and tectonic processes in area a hydrothermal vent on the Southwest Indian Ridge. *Science China Earth Sciences*, *56*(12), 2186–2197. https://doi.org/10.1007/s11430-013-4630-5

Zhao, M., Qiu, X., Li, J., Sauter, D., Ruan, A., Chen, J., et al. (2013). Three-dimensional seismic structure of the Dragon Flag oceanic core complex at the ultraslow spreading Southwest Indian Ridge (49°39′E). *Geochemistry, Geophysics, Geosystems*, *14*, 4544–4563. https://doi.org/10.1002/ggge.20264

Zhou, H., & Dick, H. J. B. (2013). Thin crust as evidence for depleted mantle supporting the Marion Rise. *Nature*, *494*(7436), 195–200. https://doi.org/10.1038/nature11842